Three-dimensional higher-order raypath separation in a shallow-water waveguide

Longyu Jiang, Zhe Zhang, Philippe Roux

Three-dimensional higher-order raypath separation in a shallow-water waveguide

Article · July 2022

DOI: 10.1121/10.0011810

3 authors, including:

Philippe Roux
University Grenoble Alpes
494 PUBLICATIONS **12,929** CITATIONS

SEE PROFILE

Three dimensional higher-order raypath separation in a shallow-water waveguide

Jiang Longyu,[1, a)] Zhang Zhe,[1] and Roux Philippe[2]

[1)] *The laboratory of Marine Information Science and Technology, School of Computer Science and Engineering, Southeast University, Nanjing 210096, China.*

[2)] *Univ. Grenoble Alpes, Univ. Savoie Mont Blanc, CNRS, IRD, Univ. Gustave Eiffel, Grenoble INP, ISTerre, 38000 Grenoble, France*

JLY@seu.edu.cn,

220151575@seu.edu.cn,

philippe.roux@univ-grenoble-alpes.fr

(Dated: 12 May 2022)

Abstract: Separating raypaths in a multipath shallow-water environment is a challenge problem due to the interferences between them and colored noise existing in ocean environment, especially for two raypaths arrive close to each other. Thus, in this paper, a three dimensional (3D) higher-order raypath separation in an array to array configuration is proposed. Performance tests using simulation data in a multipath environment, real data obtained in an ultrasonic waveguide and ocean shallow-water data, respectively, illustrate that the proposed algorithm achieves a higher resolution and a stronger robustness comparing to the existing algorithms.

[a)]Author to whom correspondence should be addressed.

1. Introduction

Acoustic rays are in multi-path propagation in a shallow-water waveguide due to the reflection and (or) the refraction by the surface of the ocean and the continental shelf. The multiple raypaths cover more parts of the ocean and provide more information than a single emitted signal. However, they also produce interferences among them. Thus, separating the raypaths is necessary in many important applications, such as passive sonar, ocean acoustic tomography[1], etc. As a classical separation algorithm, the Multiple Signal Classification (MUSIC) algorithm[2] was proposed to obtain a high-resolution separation of the sources in a point to array configuration, which is composed of a point source and a vertical receiver array. The MUSIC algorithm improves separation resolution mainly exploiting the orthogonality between the signal subspace and the noise subspace. However, it fails when the signals are fully correlated or coherent. Jiang et el.[3] proposed a smoothing active wideband MUSIC (Smoothing-MUSICAL) algorithm, which is an extension of the MUSIC algorithm to the case of separating fully correlated or coherent wideband signals by using the spatial-frequency smoothing. ~~In addition, comparing~~ to the MUSIC algorithm, the smoothing-MUSICAL algorithm improves the separation resolution through adding the arrival time of each raypath to the signal model as a new discrimination parameter. In addition to second order moment-based algorithm, applying higher-order statistics to DOA estimation has been focused on by the researchers and a group of algorithms have been developed[4–10]. These algorithms exhibit superior estimation performance due to the properties of aperture extension and noise suppression of higher-order cumulants. Recently, a wideband raypath

separation algorithm based on the fourth-order cumulant[11] ~~is~~ proposed in a point to array configuration in a shallow-water waveguide. Higher resolution and more robust separation is ~~also~~ obtained ~~while~~ at a cost of computation time. ~~Sequentially,~~ Jiang et el. propose a fast algorithm using low-rank matrix approximation[12] to reduce the computation cost of the 4-smoothing-MUSICAL algorithm. ~~On the other hand,~~ Roux et el[18] ~~develop~~ an array to array configuration, which is composed of a source vertical array and a receiver vertical array. A double-beamforming algorithm ~~is~~ introduced ~~experimentally~~ ~~in the configuration and a high-resolution tomography~~ ~~inversion~~[13] ~~is finally obtained through using its separation results.~~ ~~Moreover,~~ Touzé et el[14] present the double-capon algorithm and the double-MUSICAL algorithm under the assumption of white Gaussian noise. To further improve both the resolution and the robustness to the colored noise, we present a 3D higher-order raypath separation algorithm in an array to array configuration ~~in this paper.~~ Its performance improvement is achieved due to inheriting the merits of using both the higher-order cumulants and the array to array configuration.

The rest of the paper is organized as follows. In Section 2, we give an elaborate description of the 3D higher-order raypath separation algorithm. In Section 3, we test the performance of the proposed algorithm using simulation data in a multi-path environment, real data obtained in an ultrasonic tank and ocean data, respectively. The paper is concluded in Section 4.

2. The 3D higher-order raypath separation algorithm

2.1 Signal model

Assume the raypaths propagate in a double vertical array configuration, which is composed of an emission array (N sources) and a receiver array (M sensors). The P (P is assumed known[15,16]) raypaths at the frequency ν produced by the n^{th} source and received on the m^{th} receiver is noted as $x_{m,n,\nu}$ and modeled as follows.

$$x_{m,n,\nu} = s_\nu \sum_{p=1}^{P} a_p e^{\Phi_p} + b_{m,n,\nu} \tag{1}$$

where s_ν is the source spectrum, $\Phi_p = -j2\pi\nu(T_p + (m-m_0)\tau_p^e + (n-n_0)\tau_p^r)$, $\tau_p^e = dsin(\theta_p^e)/c$ and $\tau_p^r = dsin(\theta_p^r)/c$. T_p notes the arrival time of the p^{th} raypath. m_0 (n_0) refers to the reference source (receiver). τ_p^e (τ_p^r) is the time delay for the p^{th} raypath propagates between two adjacent sources (receivers). d is the interval between two adjacent sources (receivers). θ_p^e (θ_p^r) is the direction of emission (reception) of the p^{th} raypath. a_p notes the amplitude of the p^{th} raypath. $b_{m,n,\nu}$ refers to the additive noise.

2.2 Data model

Based on the signal model built in the above section, each signal received in the double-array configuration is a data cube for all N sources, M sensors and F frequencies of the wide-band signals considered in the algorithm. The data model is built through concatenating the data cube's elements into a long vector[19]. First, the elements corresponding to the source n^{th} at the frequency ν on all the M elements of the receiver array is concatenated into a vector as follows (+ notes transpose.) :

$$\mathbf{x}_{n,\nu} = [x_{1,n,\nu} \dots x_{M,n,\nu}]^+ \tag{2}$$

The elements corresponding to both the N source and the M sensors are further concatenated into the following vector.

$$\mathbf{x}_\nu = [\mathbf{x}_{1,\nu} \dots \mathbf{x}_{n,\nu}]^+ \tag{3}$$

Finally, considering all the F frequencies, the long vector $\mathbf{X}$ is obtained as follows.

$$\mathbf{X} = [\mathbf{x}_{\nu_1} \dots \mathbf{x}_{\nu_F}]^+ \tag{4}$$

Similarly, the steering vector $\mathbf{d}(\theta_p^e \theta_p^r, \mathbf{T}_p)$ and the additive noise $\mathbf{b}$ can be also concatenated into long vectors. Thus, the received signal in the frequency domain can be rewritten in the following matrix form.

$$\mathbf{X} = \sum_{p=1}^{P} a_p \mathbf{d}(\theta_p^e, \theta_p^r, \mathbf{T}_p) + \mathbf{b} = \mathbf{D}(\theta_p^e, \theta_p^r, \mathbf{T}_p) + \mathbf{b} \tag{5}$$

where

$\mathbf{X} = [\mathbf{x}_{\nu_1}, \mathbf{x}_{\nu_2}, \cdots, \mathbf{x}_{\nu_F}]^+$, $\mathbf{x}_\nu = [\mathbf{x}_{1,\nu}, \mathbf{x}_{2,\nu}, \cdots, \mathbf{x}_{N,\nu}]^+$ $(\nu = \nu_1, \nu_2, \cdots, \nu_F)$, and $\mathbf{x}_{n,\nu} = [x_{1,n,\nu}, x_{2,n,\nu}, \cdots, x_{M,n,\nu}]^+$ $(n = 1, 2, \cdots, N)$. $\theta_p^e = [\theta_1^e, \theta_2^e, \cdots, \theta_P^e]^+$, $\theta_p^r = [\theta_1^r, \theta_2^r, \cdots, \theta_P^r]^+$, $\mathbf{T}_p = [T_1, T_2, \cdots, T_P]^+$.

$\mathbf{d}(\theta_p^e, \theta_p^r, \mathbf{T}_p) = [\mathbf{d}_{\nu_1}(\theta_p^e, \theta_p^r, \mathbf{T}_p), \mathbf{d}_{\nu_2}(\theta_p^e, \theta_p^r, \mathbf{T}_p), \cdots, \mathbf{d}_{\nu_F}(\theta_p^e, \theta_p^r, \mathbf{T}_p)]^+$, with $\mathbf{d}_{\nu_i}(\theta_p^e, \theta_p^r, \mathbf{T}_p) = [s_{\nu_i} e^{-j2\pi\nu_i(T_p + (1-n_0)\tau(\theta_p^e))} \mathbf{d}(\theta_p^r)_{\nu_i}, \cdots s_{\nu_i} e^{-j2\pi\nu_i(T_p + (N-n_0)\tau(\theta_p^e))} \mathbf{d}(\theta_p^r)_{\nu_i}]^+$ $(i = 1, 2, \dots, F)$ and $\mathbf{d}(\theta_p^r)_{\nu_i} = [e^{-j2\pi\nu_i(1-m_0)\tau(\theta_p^r)}, \cdots, e^{-j2\pi\nu_i(M-m_0)\tau(\theta_p^r)}]^+$.

$\mathbf{b} = [\mathbf{b}_{\nu_1}, \mathbf{b}_{\nu_2}, \cdots, \mathbf{b}_{\nu_F}]^+$, with $\mathbf{b}_\nu = [\mathbf{b}_{1,\nu}, \mathbf{b}_{2,\nu}, \cdots, \mathbf{b}_{N,\nu}]^+$ $(\nu = \nu_1, \nu_2, \cdots, \nu_F)$, and $\mathbf{b}_{n,\nu} = [b_{1,n,\nu}, b_{2,n,\nu}, \cdots, b_{M,n,\nu}]^+$ $(n = 1, 2, \cdots, N)$

85 *2.3 Principle of the Algorithm*

86 Using the data model built above, the trispectrum matrix of the received signal can be
87 theoretically computed according to the following equation.

$$\begin{aligned}\mathbf{C} &= E\{(\mathbf{X}\bigotimes\mathbf{X}^*)(\mathbf{X}\bigotimes\mathbf{X}^*)^H\}\\ &-E\{(\mathbf{X}\bigotimes\mathbf{X}^*)\}E\{(\mathbf{X}\bigotimes\mathbf{X}^*)^H\}\\ &-E\{(\mathbf{X}\mathbf{X}^H)\}\bigotimes E\{(\mathbf{X}\mathbf{X}^H)^*\},\end{aligned} \tag{6}$$

88 where $*$ notes conjugate, H notes conjugate transpose and $\bigotimes$ notes kronecker product,
89 respectively. However, in a real ocean experiment, it is costly to obtain several realizations
90 for computing the expectation of the stochastic process. Moreover, the raypaths are reflected
91 or refracted by the emitted signal thus they are fully correlated or coherent, which will lead
92 to a rank deficiency of the trispectrum matrix. To resolve the problems, we use a three
93 dimensional smoothing technique[14] to generate several realizations based on the received
94 signal. The spatial-frequency smoothing algorithm has two major advantages : (1) it is easy
95 to implement; (2) it first combines the spatial and frequency smoothing to provide more
96 useful information for estimation. To completely separate all the raypaths, it is necessary to
97 select the number of sub-antennas greater than the number of raypaths[3]. The smoothing is
98 performed in the dimensions of the emitted array, the receiver array and the frequency bins,
99 respectively. That is, the emitted (receiver) array is divided into K_e (K_r) subarrays for a
100 length of $N_e^s = N - K_e + 1$ ($N_r^s = M - K_r + 1$). Similarly the K_f frequency subbands are
101 respectively composed of $N_f^s = F - K_f + 1$ frequency bins. Through these operation, we

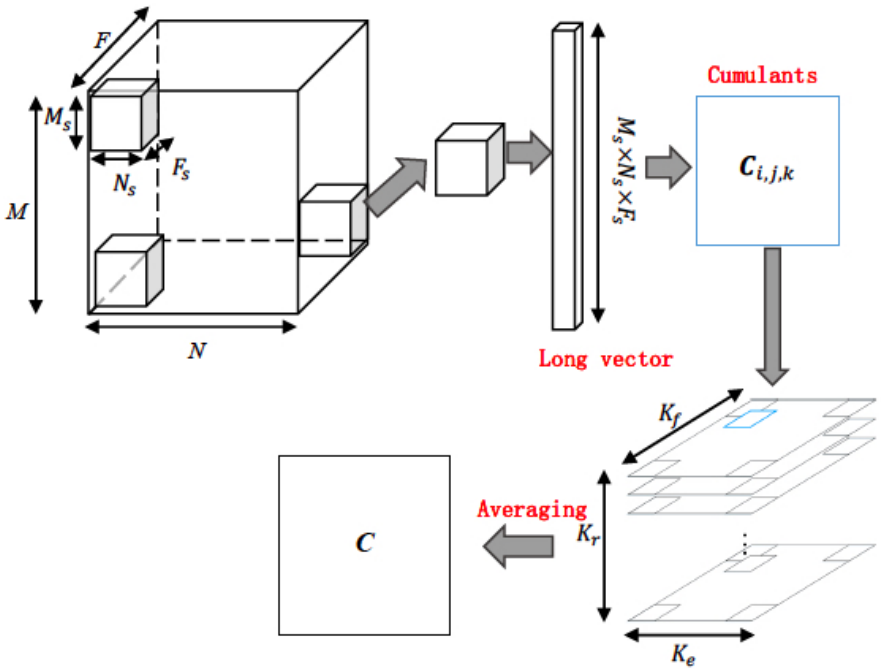

Fig. 1. Schematic diagram of the smoothing technique for the cumulants. The $\mathbf{C}$ and $\mathbf{C}_{i,j,k}$ are computed based on the long vector trough the Eq. (7). The size of the matrix $\mathbf{C}$ is equal to $(N_e^s \times N_r^s \times N_f^s)^2$.

generate $K_e \times K_r \times K_f$ small data cubes, whose dimensions are $N_e^s \times N_r^s \times N_f^s$. The $\mathbf{X}_{i,j,k}$ is obtained through connecting the elements of all the three dimensions into a long vector. To be easily understood, the schematic diagram of the smoothing technique for the cumulants is provided in Fig. 1.

The expectation of the trispectrum matrix of the received signal is finally estimated through an average of these smaller trispectrum matrices computed through the small data cubes, which is specifically described in Eq. 7.

$$\begin{aligned}\widehat{\mathbf{C}} = \frac{1}{K_e K_r K_f}\sum_{k=1}^{K_f}\sum_{j=1}^{K_e}\sum_{i=1}^{K_r}\mathbf{C}_{i,j,k} = \frac{1}{K_e K_r K_f}\sum_{k=1}^{K_f}\sum_{j=1}^{K_e}\sum_{i=1}^{K_r} E\{(\mathbf{X}_{i,j,k}\bigotimes\mathbf{X}^*_{i,j,k})(\mathbf{X}_{i,j,k}\bigotimes\mathbf{X}^*_{i,j,k})^H\} \\ -E\{(\mathbf{X}_{i,j,k}\bigotimes\mathbf{X}^*_{i,j,k})\}E\{(\mathbf{X}_{i,j,k}\bigotimes\mathbf{X}^*_{i,j,k})^H\} - E\{(\mathbf{X}_{i,j,k}\mathbf{X}^H_{i,j,k})\}\bigotimes E\{(\mathbf{X}_{i,j,k}\mathbf{X}^H_{i,j,k})^*\},\end{aligned} \tag{7}$$

Then, we apply the eigenvalue decomposition to $\widehat{\mathbf{C}}$ as follows.

$$\widehat{\mathbf{C}} = \mathbf{U}\mathbf{\Lambda}\mathbf{U}^H = \sum_{i=1}^{(N_e^s\times N_r^s\times N_f^s)^2}\lambda_i\mathbf{u}_i\mathbf{u}_i^H = \sum_{i=1}^{P^2}\lambda_i\mathbf{u}_i\mathbf{u}_i^H + \sum_{i=P^2+1}^{(N_e^s\times N_r^s\times N_f^s)^2}\lambda_i\mathbf{u}_i\mathbf{u}_i^H \tag{8}$$

where $\mathbf{U}$ is composed of $(N_e^s\times N_r^s\times N_f^s)^2$ eigenvectors, $\mathbf{\Lambda}$ is a diagonal matrix containing the $(N_e^s\times N_r^s\times N_f^s)^2$ eigenvalues and $\mathbf{u}_i$ denotes the i^{th} eigenvector. Arranging all the eigenvalues from largest to smallest $\lambda_1 > \lambda_2 > \cdots, > \lambda_{(N_e^s\times N_r^s\times N_f^s)^2}$, the $(N_e^s\times N_r^s\times N_f^s)^2 - P^2$ eigenvectors corresponding to the smallest eigenvalues project the noise subspace $\mathbf{U}_n\mathbf{U}_n^H$ where

$$\mathbf{U}_n = \left[\mathbf{u}_{P^2+1}, \mathbf{u}_{P^2+2}, \cdots \mathbf{u}_{(N_e^s\times N_r^s\times N_f^s)^2}\right] \tag{9}$$

Finally, the estimator $P_{Double\ 4-s-MUSICAL}$ in the double-array configuration can be constructed as follows.

$$P_{Double\ 4-s-MUSICAL} = \frac{1}{\mathbf{d}_4^H\mathbf{U}_n\mathbf{U}_n^H\mathbf{d}_4} \tag{10}$$

with the steering vector $\mathbf{d}_4 = \mathbf{d}(\theta_p^r, \theta_p^e, T_p)\otimes\left(\mathbf{d}(\theta_p^r, \theta_p^e, T_p)\right)^*$.

3. Performance test

In this section, the performance of the proposed algorithm is tested using simulation data in a multi-path environment, small-scale data obtained in an ultrasonic tank and ocean data[18], respectively. The test parameters used in these experiments are shown in Table 1 and Table 2. $z_{s_1} \sim z_{s_M}$ notes the depths in which the first source to the M^{th} source is fixed under the water while $z_{r_1} \sim z_{r_N}$ refers to the ranges which the first receiver to the N^{th} receiver cover. D is the distance between the reference source and the reference receiver. c indicates the acoustic velocity in which the raypaths propagate under the water. The central frequency of the emitted signal is ν_c and its bandwidth is noted as ν_w. ν_n notes the number of frequencies used in each test choosing the beginning frequency ν_b to the last frequency ν_e. N_s refers to the number of samples used in each test in the time domain.

Figures 2 and 3 show the separation results of the proposed algorithm while the contrast ones of the smoothing-MUSICAL algorithm and the 4-smoothing-MUSICAL algorithm are also provided. Specifically, figure 2 (a), (c) and (e) illustrate the separation results of a set of simulation data under the assumption that the waveguide provides nearly perfect boundary conditions at the water-bottom interface. In the case, five raypaths propagate between the double array configuration composed of four emitters and four receivers. The signal to noise ratio is equal to 2dB. The SNR is defined as the power ratio of signal to noise in the signal band. These powers are estimated in the time domain by the sum of squares of samples (signal or noise). The reference source (receiver) is located at 50m under the water. The smoothing-MUSICAL algorithm provides a two-dimensional (2D) separation

in a plan of the arrival time and the direction of arrival (DOA) in figure 2 (a) while the other two algorithms give a 3D separation with the additional parameter: the direction of emission (DOE) in figure 2 (c) and figure 2 (e), respectively. In figure 2 (a), (c) and (e), each spot corresponds to a raypath and the black crosses mark the theoretical positions. It is obviously that the smoothing-MUSICAL algorithm fails in finding the raypath with the DOA around at -5° in figure 2 (a) and the raypath with the DOA around at 0° is deficient in the results of the double-MUSICAL algorithm in figure 2 (c). In contrast, the proposed algorithm successfully separates all the five raypaths without any artifact in figure 2 (e), where the deficient raypaths in figure 2 (a) and figure 2 (c) are highlighted by the red circles.

Figure 2(b), (d) and (f) illustrate the performance contrast of the three algorithms using a set of real data obtained at a small-scale ultrasonic tank. The small-scale experiment reproduces the actual physical phenomena occurring in the real ocean environment in a smaller scale inside the laboratory based on the operation multiplying the frequency of the signals by a factor and dividing the spatial distances by the same factor. Thus, the small-scale experiment is a reduced cost and a totally controlled experiment. Specifically, in this tank, a steel bar acts as the bottom, for which the boundary conditions are nearly perfect at the water-bottom interface, and a 1.10m-long, 5.4-cm-deep acoustic waveguide is constructed[17]. Two coplanar 64-element vertical line arrays ~~(VLA) are placed and the~~ central frequency of the transducer is 1 ~~or 3~~ MHz with a 50% frequency bandwidth. The transducer dimensions $0.75mm \times 12mm$ are used to make the linear arrays omni-directional in the plane defined by the source-receiver arrays and the beams collimated in the plane perpendicular to the

159 waveguide axis. Figure 2(b), (d) and (f) show a group of separation results with a set of real
160 data obtained in the small-scale experiment. There are seven predictable raypaths in the
161 example, whose theoretical positions are indicated by the black crosses. Figures 2(b) and
162 2(d) show the separation results using the smoothing-MUSICAL algorithm and the double-
163 MUSICAL algorithm, respectively. It can be clearly seen that both of the two algorithms
164 are deficient in detecting one raypath with the DOA around at 5°. Comparing to them, the
165 proposed 3D higher order algorithm correctly find all the seven raypaths in figure 2(f), where
166 the red circle highlights the deficient raypath in figures 2(b) and 2(d).

167 Finally, the performance of the double-4-smoothing algorithm is tested using ocean
168 data. The experiment has been performed in July 2005 north of Elba Island, Italy[18]. It uses
169 a similar experimental setup to the small-scale ultrasonic experiment, although at a much
170 larger scale. Two equally spaced vertical linear arrays are implemented in 120 m water and
171 the distance between them is 4.071 km. The source array (SA) is composed of 29 transducers
172 covering 78 m and the receiver array (RA) has 32 hydrophones spanning 62m. The central
173 frequency of the transducers is 3.2 kHz with 1 kHz bandwidth. Figure 3 shows the contrast
174 of separation results using a set of ocean data, which has been acquired in a down-refraction
175 profile. There are three expected rays, a surface-reflected ray and two refracted rays. Each
176 refracted ray has a turning point near the depth of maximum sound-speed variability. Due
177 to the sound speed variation described in the Ref.[18], the three raypaths arrived at close
178 time. Figure 3(a) shows that the separation result of the smoothing-MUSICAL algorithm
179 in the plan of the arrival time and the DOA. It detects just a mixed spot for two of the

three raypaths due to their close arrival times and DOAs. Figure 3(b) shows that the separation result of the double-MUSICAL algorithm in the plan of the emitted angle and the DOA, which has a raypath deficiency with the DOA around at 10°. However, the proposed algorithm gives an accurate separation for the three raypaths shown in the plan of the emitted angle and the DOA in Figure 3 (c) because of the different emitted angles and a strong robustness of the proposed algorithm to the fluctuant ocean. Figure 3(d) displays the three raypaths in Figure 3(a)-(c), which propagate between the centers of source and receive arrays.

Moreover, we test the performance of the double-4-smoothing-MUSICAL algorithm using the simulation data at different SNRs in a red noise inference environment and compare its separation performance in terms of root-mean-square errors (RMSE) with that of the double-MUSICAL algorithm. In these Monte Carlo experiments, we define the average RMSE of the 3D separation result $\hat{R}_p$ for the p^{th} raypath as follows.

$$RMSE_{R_p} = \sqrt{\frac{1}{K_p}\sum_{k=1}^{K_p} \|\hat{R}_p - R_p\|^2} \tag{11}$$

where K_p is the number of the trials, which is equal to 20 for these Monte Carlo experiments. That is, the simulations are performed 20 times at each different SNR. 400 simulations in total are performed in red noise environments with their SNRs ranging from -20 dB to 20 dB. The configuration parameters used in the simulations are consisted with those shown in Table I and Table II. For those raypaths which can be separated by both the two algorithms, the RMSEs are computed at each dimension of the 3D separation result. Specifically, figures

	M	N	$z_{s_1} \sim z_{s_M}(m)$	$z_{r_1} \sim z_{r_N}(m)$	d (m)
Simulation	4	4	$47.5 \sim 52.5$	$47.5 \sim 52.5$	2.5
Small-scale experiment	4	5	$26.375 \times 10^{-3} \sim 28.625 \times 10^{-3}$	$25.625 \times 10^{-3} \sim 28.625 \times 10^{-3}$	0.75×10^{-3}
Ocean data	4	4	$93.098 \sim 101.456$	$94 \sim 100$	2

Table 1. The configuration parameters of simulation, small-scale experiment and the at-sea experiment.

4 (a), (b) and (c) show the curves of the average RMSEs for the DOE, the DOA and the time of arrival (TOA) produced by the two algorithms, respectively. In figure 4 (a), the double-4-MUSICAL algorithm generally produces a smaller bias in the low SNR range (from -20dB to 0dB) and a relatively stable performance in moderate-to-high SNR. For the average RMSEs shown in the Figures 4(b) and 4(c), the double-4-MUSICAL algorithm generally shows a better and stable performance. Based on the performance contrasts with the simulation data, small-scale data and ocean data, a conclusion is drawn that the double-4-smoothing-MUSICAL algorithm enables to achieve an aperture extension, a stronger robustness to the fluctuant environment and a resolution improvement for the extension of cumulants-based algorithm to the double-array configuration.

4. Conclusion

In this paper, we extended a higher-order algorithm to a double-array configuration. Higher-resolution and more robust separation for close arrivals even in a fluctuant ocean environment

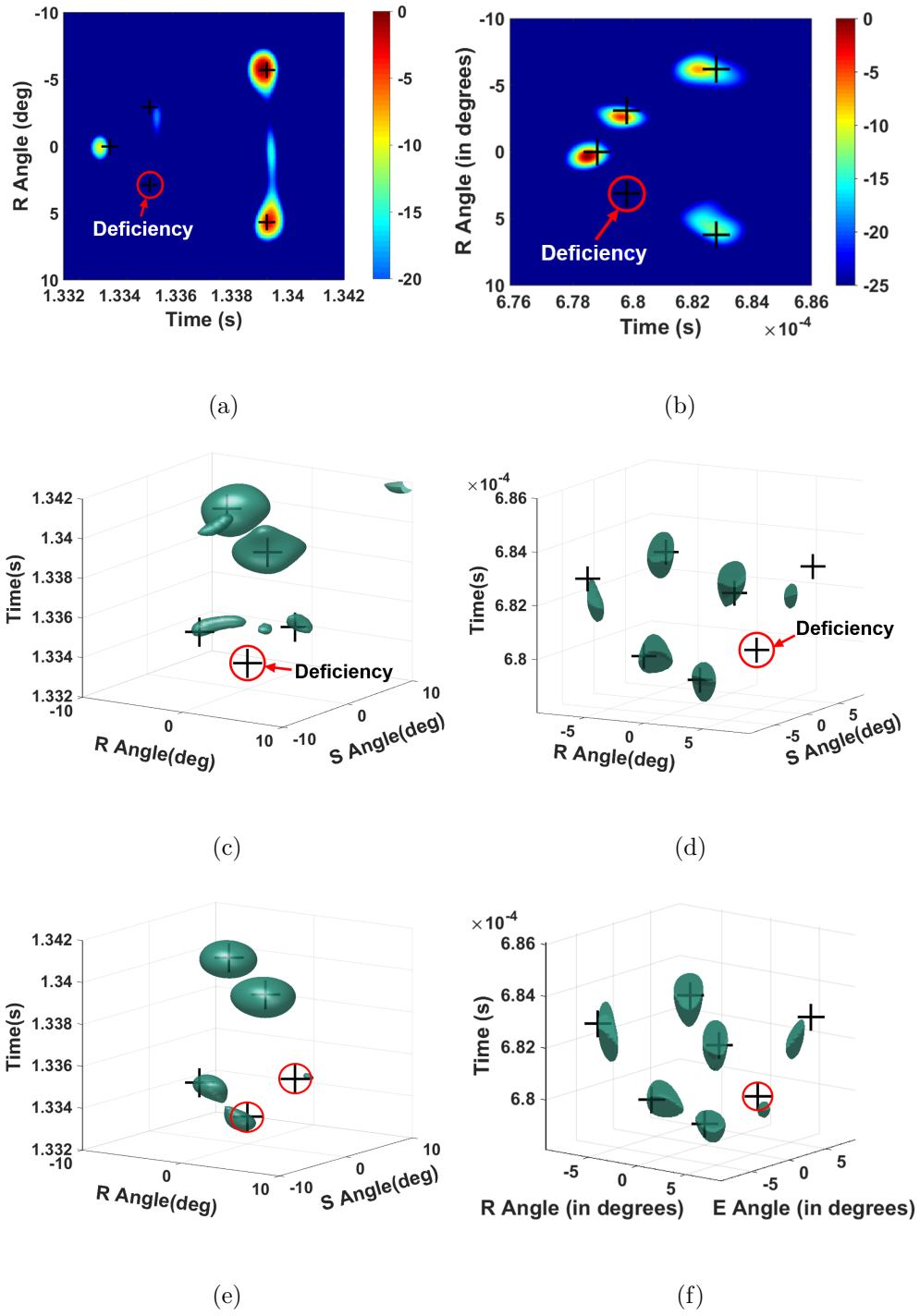

Fig. 2. Separation results comparison of different algorithms using simulation datas ((a), (c) and (e)) or using real data obtained in an ultrasonic tank ((b), (d) and (f)). The black crosses denote the theoretical values. The red circles highlight the raypaths used to differentiate the separation ability of the algorithms. (a) and (b) show the results of the smoothing-MUSICAL algorithm; (c) and (d) show the results of the double-MUSICAL algorithm; (e) and (f) show the results of the double-4-MUSICAL algorithm (The iso-surfaces are located at max-value/3.)

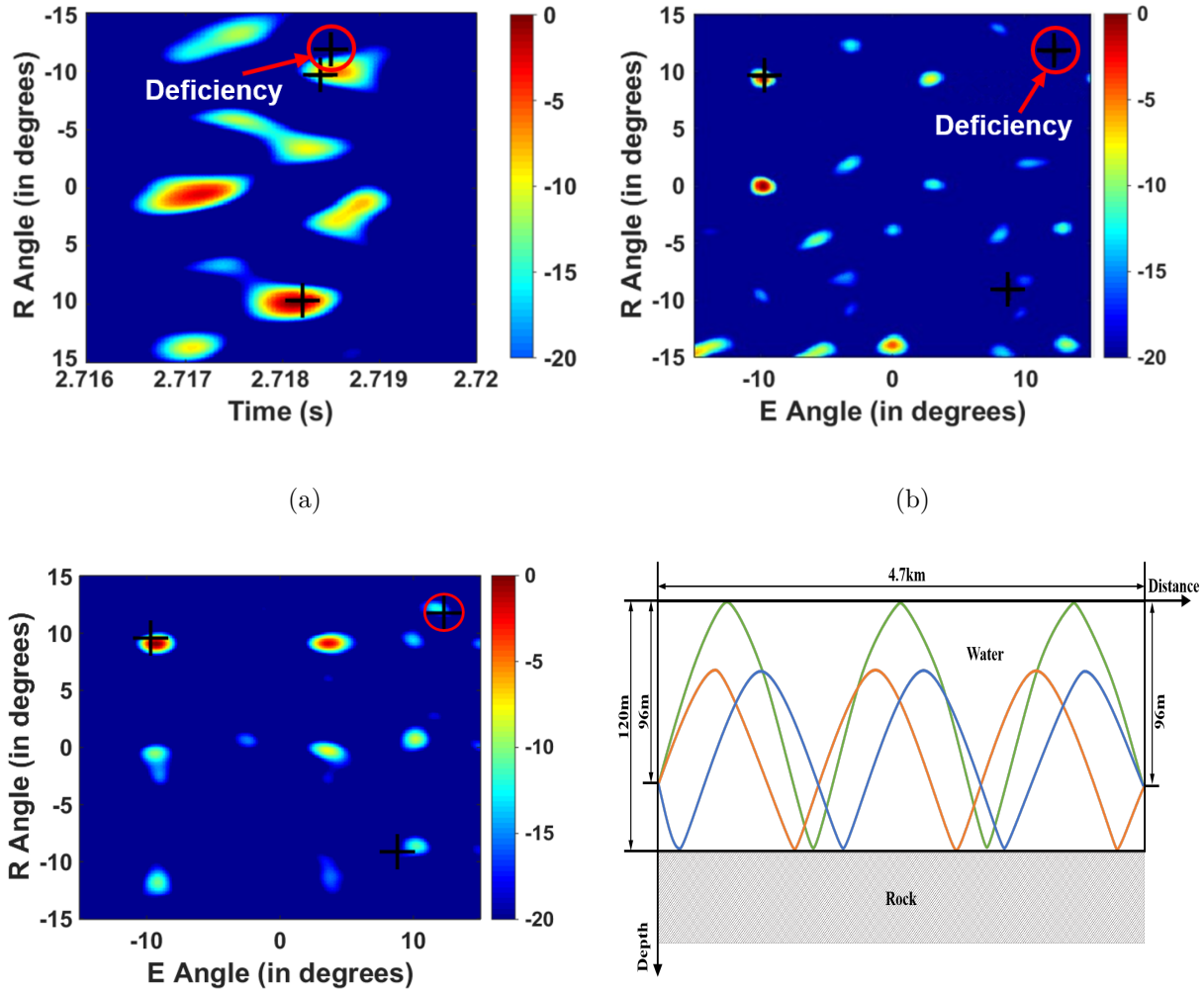

(a) (b)

(c) (d)

Fig. 3. Separation results comparison of different algorithms using ocean datas. The black crosses denote the theoretical values. The red circles highlight the raypaths used to differentiate the separation ability of the algorithms (a) the smoothing-MUSICAL algorithm; (b) the double-MUSICAL algorithm; (c) the double-4-MUSICAL algorithm; (d) Raypaths between the source and the reference sensor for the three rays.

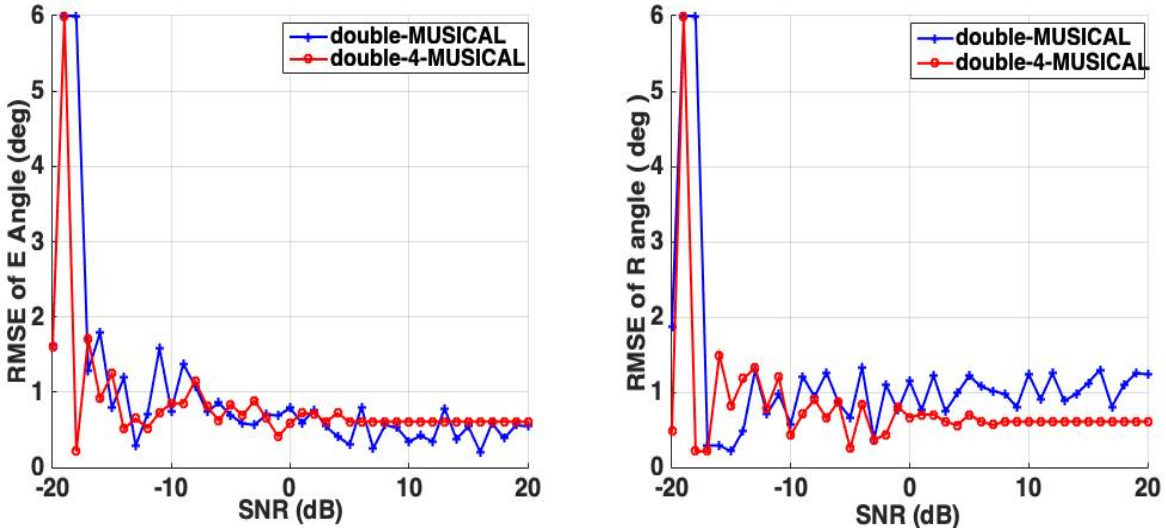

(a) (b)

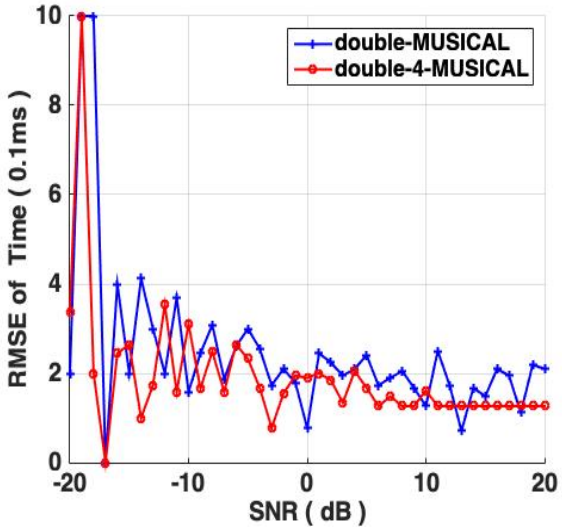

(c)

Fig. 4. The RMSE comparison of different algorithms using simulation data interfered by red noise. (a) the RMSE (in degree) of the direction of emission (DOE) vs SNR variation ; (b) the RMSE (in degree) of the direction of arrival (DOA) vs SNR variation; (c) the RMSE (in 0.1ms) of the time of arrival (TOA) vs SNR variation.

	ν_c (Hz)	ν_w (Hz)	$\nu_n(\nu_b \sim \nu_e)$ (Hz)	N_s	$D(m)$	c (m/s)
Simulation	1.5×10^3	5×10^3	75 $(0 \sim 5 \times 10^3)$	135	2000	1500
Small-scale experiment	1.2×10^6	5×10^6	$150(0 \sim 5 \times 10^6)$	132	1	1473
Ocean data	3.2×10^3	6×10^3	50 $(0 \sim 6 \times 10^3)$	60	4.701×10^3	1509

Table 2. The test parameters used in the simulations, the small-scale experiment and the at-sea experiment.

is achieved by the higher-order 3D algorithm. In future work, we will study the inversion for ocean acoustic tomography based on the separation results.

Acknowledgments

This resarch has been supported by the National Natural Science Foundation of China (Nos. 61871124 and 61876037), the State Key Laboratory of Acoustics, Chinese Academy of Sciences (No. SKLA201604), and the Scientific Research Foundation for the Returned Overseas Chinese Scholars. The Focused Acoustic Forecasting experiment (FAF05) experiment was performed in collaborative experiments with the NATO Underwater Research Centre (NURC), La Spezia, Italy, with Mark Stevenson as Chief Scientist. Scientists who contributed to these experiments include Tuncay Akal, W. A. Kuperman, W. H. Hodgkiss, H.C. Song, B.D. Cornuelle, Piero Boni, Piero Guerrini, other NURC staff, and the officers and crew of the RV Alliance. ISTerre is part of Labex OSUG@2020. .

References and links

[1]W.H. Munk, and P. F. Worcester. "Ocean acoustic tomography", *Oceanography*, vol.1, no. 1, pp. 8-10, 1988.

[2]R. Schmidt, " Multiple emitter location and signal parameter estimation," *IEEE Transactions on Antennas and Propagation*, vol. 34, no. 3, pp. 276-280, 1986.

[3]L. Jiang, P. Roux, and J. I. Mars, " Raypath separation with a high-resolution algorithm in a shallow-water waveguide," *IEEE Journal of Oceanic Engineering*, vol. 43, no. 1, pp. 119-130, 2018.

[4]Y. H. Chen and Y. S. Lin, "Doa estimation by fourth-order cumulants in unknown noise environments," *IEEE International Conference on Acoustics, Speech, and Signal Processing*, vol. 4, pp. 296-299, 1993.

[5]M. C. Dogan and J. M. Mendel, "Applications of cumulants to array processing. I. Aperture extension and array calibration," *IEEE Trans. Signal Processing*, vol. 43, no. 5, pp.1200-1216,1995.

[6]M. C. Dougan and J. M. Mendel, "Applications of cumulants to array processing. II. Non-Gaussian noise suppression," IEEE Trans. Signal Processing, vol. 43, no. 7, pp.1663-1676 ,1995.

[7]E. Gonen, J. M. Mendel, and M. C. Dogan, "Applications of cumulants to array processing. iv. direction finding in coherent signals case," IEEE Trans. Signal Processing, vol. 45, no. 9, pp. 2265-2276,1997.

[8]P. Chevalier, A. Ferreol, and L. Albera, "High-resolution direction finding from higher order statistics:The 2q-music algorithm," IEEE Trans. Signal Processing, vol. 54, no. 8, pp. 2986-2997, 2006.

[9]G. Birot, L. Albera, and P. Chevalier, "Sequential high-resolution direction finding from higher order statistics," IEEE Trans. Signal Processing vol. 58, no. 8, pp. 4144-4155, 2010.

[10]P. Pal and P. Vaidyanathan, "Multiple level nested array: An efficient geometry for 2qth order cumulant based array processing," IEEE Trans. Signal Processing, vol. 60, no. 3, pp. 1253-1269, 2012.

[11]L. Jiang, Y. Hong, P. Roux, J. Wu, and H. Shu, " Active wideband higher-order raypath separation in multiple environment," *The Journal of the Acoustical Society of America*, vol. 141, no. 1, pp. EL38-EL44, 2017.

[12]L. Jiang, W. Song, Z. Zhang, C.Yang, S. Wang, and P. Roux, "Fast raypath separation based on low-rank matrix approximation in a shallow-water waveguide," *The Journal of the Acoustical Society of America*, vol. 143, no. 1, pp. EL271-EL278, 2017.

[13]I. Iturbe, P. Roux, B. Nicolas, and J. Mars, "Ocean acoustic tomography using a double-beamforming algorithm" *IEEE Journal of Oceanic Engineering*, vol. 123, no. 5, pp. 3912-EL278, 2008.

[14]G. Touzé, B. Nicolas, J. Mars, P. Roux, B. Oudompheng "Double-Capon and double-MUSICAL for arrival separation and observable estimation in an acoustic waveguide," *Eurasip Journal on Advances in Signal Processing*, vol. 143, no. 1, pp. EL271-EL278, 2017.

[15]L. Jiang and J. I. Mars, "Automatic detection of the number of raypaths in a shallow-water waveguide, " *IEEE Journal of Oceanic Engineering*, vol. 39 (4): 713-723, 2014.

[16]M. Wax and T. Kailath, Detection of signals by information theoretic criteria, *IEEE Trans. Acoust. Speech Signal Process.*, vol. 33, no. 2, pp. 387-392, 1985.

[17]Roux P and Nicolas B, "Inverting for a deterministic surface gravity wave using the sensitivity-kernel approach", *Journal of the Acoustic Society of America*, vol.135, no. 4, pp. 1789-1799, 2014.

[18]Roux P., Cornuelle B. D., Kuperman W. A, WS Hodgkiss, "The structure of raylike arrivals in a shallow-water waveguide", *The Journal of the Acoustical Society of America*, vol.124, no. 6, pp. 3430-3439, 2008.

[19]C. Paulus, P. Gounon, and J. I. Mars, "Wideband spectral matrix filtering for multicomponent sensors array," *Signal Process.*, vol. 85, no. 9, pp. 1723-1743, 2005.